Multiband electron resonant Raman scattering in quantum wells in a magnetic field

V. López-Richard and G.-Q. Hai
Instituto de Física de São Carlos, Universidade de São Paulo, 13560-970, São Carlos, São Paulo, Brazil

C. Trallero-Giner
Departamento de Física Teórica, Universidad de La Habana, San Lázaro y L, 10400, La Habana, Cuba

G. E. Marques
Departamento de Física, Universidade Federal de São Carlos, 13565-905, São Carlos, São Paulo, Brazil
(Received 19 July 2002; revised manuscript received 20 December 2002; published 28 April 2003)

A theoretical model has been developed for the electronic resonant Raman scattering processes in direct band zinc blende–type semiconductor quantum wells in a magnetic field. In order to take into account the spin-flip transitions, anomalous behavior of the Landau levels and the Landè g factor, an 8×8 Kane-Weiler Hamiltonian model has been considered for the evaluation of the Raman scattering amplitude. Elements concerning the selection rules of resonant inelastic light scattering in quantum well systems are reported. The multiband model predicts conditions for resonant spin-flip Raman processes in several light scattering configurations for crossed and parallel polarization. Special emphasis is given to the effects of the interlevel coupling and mixing within the conduction subband and their relation to spin-flip and inter-Landau level transitions. Symmetry and electronic properties of the level structure in the first conduction subband as well as anomalous Landè factors are discussed in terms of complementary Raman scattering configurations, Fermi energy, and multiband parameters.

DOI: 10.1103/PhysRevB.67.155320 PACS number(s): 78.30.Fs, 73.21.Fg

I. INTRODUCTION

A detailed calculation of the electronic resonant Raman scattering (ERRS) cross section in bulk semiconductors and two-dimensional electron systems has often been considered a a tedious task.[1] The basic ideas related to the electronic Raman scattering calculation in doped bulk semiconductors under external magnetic field have already been established (see Ref. 2 and references therein). The electron-electron interaction, collective excitation, spin wave, and energy band nonparabolicity effects on the Raman cross section were analyzed in Refs. 2–5. Also, the role of the complex band structure and its influence on spin-flip transitions was stressed by Blum in Ref. 1, where general features and major improvements to the ERRS microscopic theory for real semiconductors in a magnetic field were established. From the above general formalism and in a natural way it was shown that for the scattering light wave vector parallel to the direction of the magnetic field, the spin-flip excitation is an allowed process because the band coupling does not necessarily conserve the spin. Also, it becomes clear that inter-Landau-level transitions ($\Delta N_e \neq 0$) contribute to the scattering cross section even in the dipole approximation, a forbidden result in the framework of a simple parabolic model.

Usually nonresonant Raman scattering theory is exploited to explain experimental data in quantum wells (QW's), which are obtained in resonant conditions.[6] Recently, ERRS was studied theoretically by Wang and Das Sarma for one-dimensional (1D), 2D, and 3D semiconductor systems within parabolic band structures.[7] In their study, following the pioneering works on the field,[1–5] the electron-electron interaction was considered within the random-phase approximation for the electron gas in the conduction band. It was shown that the Raman spectral weight of single-particle excitations was significantly enhanced in the resonant Raman scattering condition. Under resonant conditions $E_g \lesssim \hbar\omega_L$ (E_g being the effective energy gap and ω_L the incoming light frequency), it is necessary to consider the interband transitions to describe the electronic Raman scattering. As we mentioned above, however, the nonresonant theory that ignores the role of the valence band on the ERRS processes discards important aspects concerning relative Raman intensities, optical selection rules in different scattering geometries, and their relation to the symmetry properties of the electronic structure of both conduction and valence bands.[1,8] Here, we report a resonant microscopic theoretical model for the scattering cross section where the detailed effects of the complexity of the band structure are included and only transitions of single particle nature are taken into account. Formally, our theoretical calculation can be considered as an extension of the former ERRS theory in semiconductors in a magnetic field to quasi-two-dimensional heterostructures or QW's. Nevertheless, we have implemented a direct calculation of the Raman scattering cross section and the corresponding selection rules for different scattering configurations taking into account the detailed multiband structure according to the 8×8 $\mathbf{k}\cdot\mathbf{p}$ Hamiltonian model.

We emphasize that a simple parabolic band model is unable to explain the complex response of the system in different inelastic light scattering configurations. Despite a large amount of theoretical and experimental work devoted to ERRS in bulk semiconductors[2,9,10] or intrasubband and intersubband Raman scattering processes in quantum wells,[7,11–15] there are no clear references to proper theoretical detailed calculations of the magneto ERRS cross section in the resonant regime considering the complexity of the band struc-

ture. One of the main difficulties in a theoretical simulation of Raman scattering processes in magnetic fields by a resonant theory is the impossibility of explaining inter-Landau level transitions in the same QW subband without phonon assistance in the framework of the standard parabolic band theory. In this work we show that by going some steps beyond the parabolic band model and standard optical dipole approximation, the break-down of selection rules can be explained. This will allow for resonant spin-flip transitions in the same QW subband which would be forbidden otherwise. A multiband model should appear as a dominant factor in the calculation and in the interpretation of the Raman scattering cross section measurements. In particular, resonant spin-flip transitions in QW's are naturally obtained when the lack of inversion symmetry in the zinc blende structure is taken into account. The break-down of spatial parity leads to mixing of states with different spin orientations whose effects are enhanced by the proximity of conduction and valence bands. Major attention will be given in this paper to the study of electronic properties within the conduction subbands by spin-flip Raman scattering as a relevant and current topic of research.[16–18] Spin-flip Raman scattering processes have been studied intensively in narrow gap semiconductor systems, such as $Hg_{1-x}Cd_xTe$ ternary alloys.[19–21] This was a promising material for spin-flip lasers with fine magnetic field tuning mechanism. Spin-flip lasers based on narrow gap structures have been studied and used ever since. In particular, the construction of lasers with epitaxial layers of $Hg_{1-x}Cd_xTe$ allowed for an optimization in size of the devices as shown in Ref. 22.

We will focus our attention on $Hg_{1-x}Cd_xTe$/CdTe QW's since they provide a valuable system to explore the effects of electronic band structure on the Raman scattering cross section. Recent experimental and theoretical studies on layered structures based on $Hg_{1-x}Cd_xTe$ have reported new characteristics of these systems and new approaches to study their peculiar structure.[23,24] We should point out that all the physical properties studied within this work and the conclusions derived from the theoretical calculations are applicable, in principle, to several III-V or II-VI semiconductor QW's of the zinc blende energy band structures. Narrow gap ternary alloys such as $In_{1-x}Ga_xSb$, $In_{1-x}As_xP$, $Hg_{1-x}Zn_xTe$, may show similar behaviors, however, there is no restriction to apply the same qualitative analysis to other systems since the derivation and the subsequent discussion are based on pure symmetry considerations. Thus, the conclusions and the insight of the reported effects on spin-flip resonant Raman scattering are quite general and independent on the choice of the zinc blende–type material.

A special issue of the present paper is to explore different scattering configurations and to extract complementary information about the electronic structure such as Landè g factors in the QW among others, provided by different resonant spectra. Also, an analysis of the cross section dependence on the Landau level filling factor has been introduced in order to characterize the spin-dependent nature of the resonant transitions.

This paper is organized as follows. In Sec. II the ERRS is described in terms of the scattering cross section given by a second order expansion of the electron-light interaction. The wave functions and eigenvalues, as obtained for the 8×8 Hamiltonian model, are given in Sec. III. It is shown that the lack of inversion symmetry induces a coupling between different QW subbands and the carrier wave functions. Selection rules are obtained in Sec. IV for different scattering configurations. Approximations of different orders on the light wave vector are described in Secs. IV A and IV B. Section V is devoted to the general discussion and numerical results. Also we provide a direct method to measure the effective Landè factor of the first conduction subband. The conclusions are presented in Sec. VI.

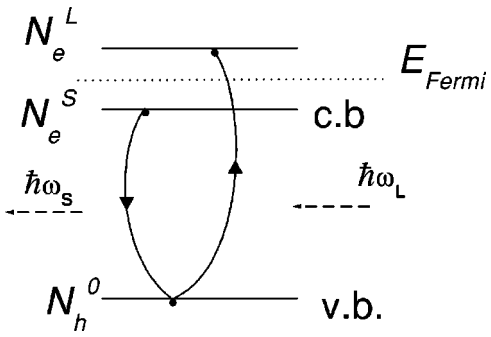

FIG. 1. Diagram representing an ERRS process. N^0 is a Landau level in the valence band and N^L and N^S are Landau levels in the conduction band. $E_{\rm Fermi}$ is the Fermi level.

II. THEORY

At low temperature the effective momentum transfer from elementary excitations to the incident light is negligible, thus in the following, we will focus our attention on the Stokes ERRS only. The system under consideration consists of a QW in a constant magnetic field B_0 along the QW growth direction (taken as the z axis). We assume the presence of a quasi-two-dimensional electron gas with density $n_{2\,\rm D}$ in the conduction band. In the partially filled conduction band in a magnetic field, the level filling can be characterized by a factor $\nu=2\pi\lambda^2 n_{2\,\rm D}$, where $\lambda=\sqrt{\hbar c/eB_0}$ is the magnetic length. The ERRS is effective at energies of the incident light $\hbar\omega_L$ larger than the effective energy gap E_g, leading to electron-hole pair creation and its subsequent annihilation. Under this condition, interband optical transitions in the QW are provoked. Our attention is focused on Raman processes, which consist of two steps. First, an incident light quantum is absorbed creating an electron-hole pair between the state N^0 in the valence band and the state N^L in the conduction band above the Fermi level. Second, a scattered photon is emitted due to an electronic transition from the state N^S below the Fermi level in the conduction band to the level N^0 at the valence band. The final state of the process consists of an electron-hole pair in the conduction band electron gas and a scattered light with energy $\hbar\omega_S$. A typical diagram of the ERRS here considered is shown in Fig. 1. Hence, neglecting the electron-phonon interaction, the ERRS process can be treated within the standard second order perturbation theory- for the heterostructure-radiation interaction V.

The Raman cross section is given by

$$\frac{d^2\sigma}{d\Omega d\omega_S}=\frac{V_0}{(2\pi)^3}\frac{\omega_S^3\eta_L\eta_S}{\omega_L c^4}\sum_{n,m}P_{nm}, \tag{1}$$

where η_L (η_S) is the refractive index at frequency ω_L (ω_S), c the light velocity, V_0 the scattered volume, and P_{nm} the transition probability per unit time between electron-hole pair states with energies E_n and E_m. The sum in Eq. (1) runs over all states that may contribute to the given process. The function P_{nm} is given by

$$P_{nm}=\frac{dw_{nm}}{dt}[g(E_m)-g(E_n)] \tag{2}$$

and within the Fermi golden rule

$$\frac{dw_{nm}}{dt}=\frac{2\pi}{\hbar}|W_{nm}(\omega_L,\omega_S)|^2\delta(E_n-E_m-\hbar[\omega_L-\omega_S]), \tag{3}$$

where $W_{nm}(\omega_L,\omega_S)$ is the scattering amplitude and $g(E_n)$ the electron-hole pair occupation probability function at energy E_n. Neglecting higher order contributions on the interaction V, there are 16 topologically nonequivalent Feynman diagrams contributing to the scattering amplitude W_{nm}. Under resonant conditions $\hbar\omega_L\gtrsim E_g$, only two terms effectively contribute to the Stokes Raman process and the scattering amplitude can be cast as

$$W_{nm}(\omega_L,\omega_S)=\sum_f\left\{\frac{V_{nf}^L V_{fm}^{+S}}{E_f-E_m+\hbar\omega_S-i\gamma}+\frac{V_{nf}^{+S}V_{fm}^L}{E_f-E_m-\hbar\omega_L-i\gamma}\right\}, \tag{4}$$

with V_{fm}^L and V_{fm}^{+S} being the optical matrix elements of the electron-hole transition $|f\rangle\rightarrow|m\rangle$ due to incident (L) or scattered (S) light, respectively, and γ accounts for the energy level broadening.

Depending on which denominators in Eq. (4) vanish, two types of resonances are present: outgoing or incoming, for the first or second term on the right-hand side of Eq. (4), respectively. For outgoing resonances photon emission takes place before photon absorption as is indicated by the first term on the RHS of Eq. (4). Thus, they would play a role in the ERRS if hole plasma in the valence band is present or at sufficiently high temperatures. Therefore, at $T\simeq 0$ K or no hole gas, outgoing resonances are disregarded and the incoming ones are the only active process reducing the probability per unit time to

$$\frac{dw_{nm}}{dt}=\frac{2\pi}{\hbar}\left|\frac{V_{nf}^{+S}V_{fm}^L}{E_f-E_m-\hbar\omega_L-i\gamma}\right|^2\delta(E_n-E_m-\hbar[\omega_L-\omega_S]), \tag{5}$$

where the delta function in Eq. (5) can be taken as a Lorentzian. If the electron-hole correlation (excitonic effect) is disregarded, the probability distribution function $g(E_n)$ of the electron-hole pair can be treated in terms of the one particle representation through the Fermi distribution function $f(E_c)$ and $f(E_v)$ for the carriers in the conduction and valence bands, respectively. For a totally filled valence band and a partially filled conduction band, we obtain for the total probability of the ERRS process

$$P=\sum_{n,m}P_{nm}=\frac{2}{\hbar}\sum_{n_e,n_{e'}}\left|\sum_{n_h}\frac{V_{n_h n_{e'}}^{+S}V_{n_e n_h}^L}{\varepsilon_{n_e}-\varepsilon_{n_h}-\hbar\omega_L-i\gamma}\right|^2 \times\frac{\gamma[f(\varepsilon_{n_{e'}})-f(\varepsilon_{n_e})]}{(\varepsilon_{n_e}-\varepsilon_{n_{e'}}-\hbar[\omega_L-\omega_S])^2+\gamma^2}, \tag{6}$$

where ε_{n_e} (ε_{n_h}) is the one-particle electronic state energy at the conduction (valence) band with a set of quantum numbers n_e (n_h).

In the following we shall study the behavior of the Raman lines as function of the Raman shift $\varepsilon_{\text{shift}}=\hbar(\omega_L-\omega_S)$, QW parameters, magneto-Raman scattering configurations, applied magnetic field, and filling factor. This can be done according to the two resonant conditions in expression (6): $\hbar\omega_L=\varepsilon_{n_e}-\varepsilon_{n_h}$ and $\hbar(\omega_L-\omega_S)=\varepsilon_{n_e}-\varepsilon_{n_e}$.

III. WAVE FUNCTIONS

The electronic structure of a zinc blende semiconductor QW in a magnetic field can be described by an 8×8 $\mathbf{k}\cdot\mathbf{p}$ Hamiltonian model.[25] Disregarding the warping terms the space of solutions can be separated into two orthogonal subspaces I and II. The wave function can be cast as[26,27]

$$|m,N_i,\mathrm{I(II)}\rangle=|k_y\rangle\begin{pmatrix}|A_1^i(B_1^i)\rangle|N-1\rangle|u_1\rangle\\ |A_2^i(B_2^i)\rangle|N-2\rangle|u_2\rangle\\ |B_3^i(A_3^i)\rangle|N-1\rangle|u_3\rangle\\ |B_4^i(A_4^i)\rangle|N-1\rangle|u_4\rangle\\ |B_5^i(A_5^i)\rangle|N\rangle|u_5\rangle\\ |B_6^i(A_6^i)\rangle|N+1\rangle|u_6\rangle\\ |A_7^i(B_7^i)\rangle|N\rangle|u_7\rangle\\ |A_8^i(B_8^i)\rangle|N\rangle|u_8\rangle\end{pmatrix}, \tag{7}$$

where i is the band index corresponding to $e\uparrow$, $hh\uparrow$, $lh\uparrow$, $so\uparrow$, $e\downarrow$, $hh\downarrow$, $lh\downarrow$, $so\downarrow$, respectively, related to the character of the main Bloch function component at $B_0=0$, $m=1,2,3,\ldots$ the subband index due to spatial quantum confinement, k_y the y component of the carrier wave vector, and $|u_j\rangle$ the set of Bloch functions at the center of the Brillouin zone given in the following order: $|u_{e\uparrow}\rangle,|u_{hh\uparrow}\rangle,|u_{lh\uparrow}\rangle,|u_{so\uparrow}\rangle,|u_{e\downarrow}\rangle,|u_{hh\downarrow}\rangle,|u_{lh\downarrow}\rangle,|u_{so\downarrow}\rangle$ for $j=1,2,\ldots,8$, respectively. $|N\rangle$ is the quantum oscillator wave function with Landau level index N describing the interaction with the magnetic field. Functions $|A_j^i\rangle$ ($|B_j^i\rangle$) are even (odd) functions of the QW without magnetic field along the z direction.

From Eq. (7) it comes implicitly that in the framework of 8×8 Hamiltonian model the magnetic field induces the coupling of different Landau levels in different bands. Thus, $N_i=0,1,2,\ldots$, labels the new Landau levels for each carrier i. Since our discussion will be focused on the lowest sub-

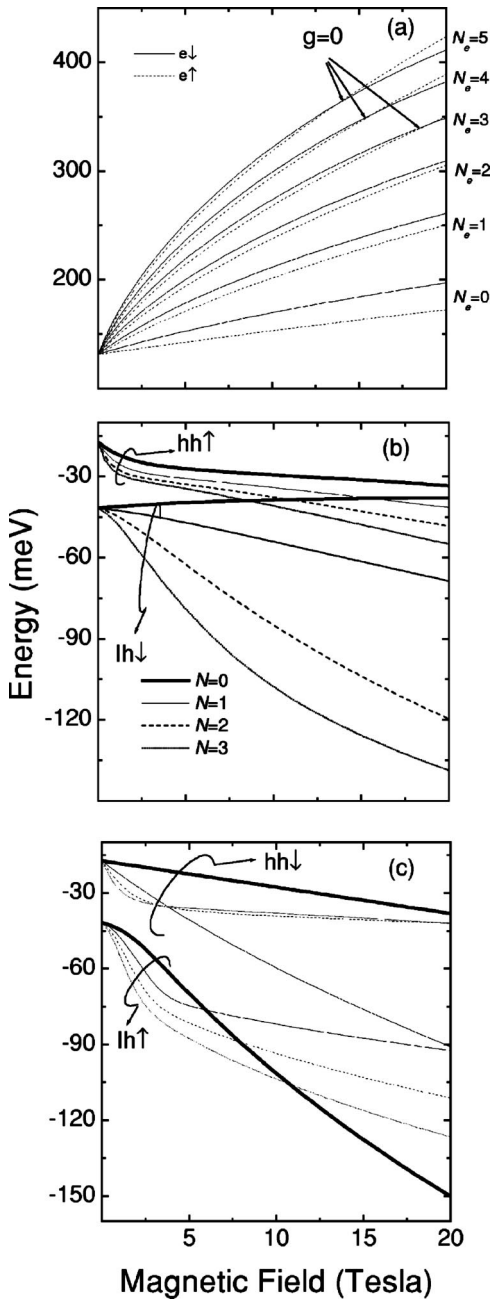

FIG. 2. Landau levels in the first subband for (a) electrons in the conduction band, (b) heavy hole spin up and light hole spin down in the valence band, and (c) heavy hole spin down and light hole spin up. For the calculation the parameters of $Hg_{0.8}Cd_{0.2}Te/CdTe$ QW of width 100 Å are chosen.

bands in each band, with $m=1$, the subband index will be dropped. The indexes n_e and n_h in Eq. (6) are replaced by the new set N_i regarding the character of the given state. In the following, in order to illustrate the strong influence of the band coupling and nonparabolicity effects on the ERRS spectra, we select the $Hg_{1-x}Cd_xTe/CdTe$ QW which presents a variable gap with Cd concentration. Nevertheless, the method and calculations are valid for any II-VI or III-V semiconductor QW.

In Fig. 2 we show Landau levels $N_{e\uparrow\downarrow}$, $N_{hh\uparrow\downarrow}$, $N_{lh\uparrow\downarrow}$ of the first subband for the conduction and valence bands, respectively. In the calculation, the same parameters were used as given in Ref. 26. Figure 2(a) shows the crossing of the levels (indicated in the figure as $g=0$) with different spin orientations leading to an inversion of the sign of the effective Landè factor. This effect has a strong influence on the ERRS as will be shown in Sec. V. The strong interlevel coupling in the valence subband is revealed in Figs. 2(b) and 2(c), where states belonging to the same solution subspace are plotted together. The strong anticrossings of coupled levels seen in the figure remark the hybridized character of heavy and light hole states. This has far reaching consequences on the ERRS selection rules. The hybridized levels contain components of their coupled neighbors which allow for transitions that would be forbidden in a simple uncoupled band model.

Using the functions given by Eq. (7), one can write the transition matrix elements explicitly as

$$\begin{aligned}\langle N_{i'''}|V^{+S}|N_{i''}\rangle\langle N_{i'}|V^{L}|N_i\rangle &= \Lambda_0 \sum_{j,j',j'',j'''=1}^{8} \langle F^{i'''}_{j'''}|e^{-i\kappa^S_z z}|F^{i''}_{j''}\rangle\langle F^{i'}_{j'}|e^{i\kappa^L_z z}|F^{i}_{j}\rangle \\ &\times\langle N^{j'''}|e^{-i\kappa^S_x x}|N^{j''}\rangle\langle N^{j'}|e^{i\kappa^L_x x}|N\rangle\langle u_{j'''}|\mathbf{e}^*_S\cdot\mathbf{p}|u_{j''}\rangle \\ &\times\langle u_{j'}|\mathbf{e}_L\cdot\mathbf{p}|u_j\rangle\,\delta_{k'''_y,k''_y-\kappa^S_y}\delta_{k''_y,k_y+\kappa^L_y},\end{aligned} \tag{8}$$

where

$$\Lambda_0=\frac{e^2}{m_0^2}\,\frac{2\pi\hbar}{V_0}\,\frac{1}{\sqrt{\omega_L\omega_S}\,\eta_L\,\eta_S},$$

where $\boldsymbol{\kappa}^{L(S)}$ and $\mathbf{e}_{L(S)}$ are the wave vector and polarization of the incident (scattered) light, respectively, N^j denotes the different Landau indexes appearing in Eq. (7), and F^i_j are the corresponding functions (A^i_j or B^i_j) along the z direction. The components of the wave vector for the incident $\boldsymbol{\kappa}^L$ and scattered $\boldsymbol{\kappa}^S$ light inside the sample are relative to the QW growth direction with a certain angle θ for which $\kappa^{L(S)}_\perp=\kappa^{L(S)}\sin\theta$ and $\kappa^{L(S)}_z=\kappa^{L(S)}\cos\theta$. The actual incident angle can be determined from the Snell law.

IV. SELECTION RULES

Let us assume the Landau level N^0_h in the first valence subband and the levels N^L_e and N^S_e in the first conduction subband with energies $\varepsilon_e(N^L_e)$ and $\varepsilon_e(N^S_e)$, respectively. Let N^L_e the state in the conduction band involved in the absorption of the incident photon and N^S_e the state from which the emission of the scattered photon occurs (see diagram in Fig. 1). For a Stokes Raman scattering process, we have $\varepsilon_e(N^L_e)>\varepsilon_e(N^S_e)$ since $\hbar\omega_L>\hbar\omega_S$ and the same valence band level is involved in the absorption and emission of photons. For transitions within the first conduction and first valence subband ($m=1$) one can guarantee, within a wide range of magnetic fields, that

$$\varepsilon_e(N^L_e)\geqslant\varepsilon_e(N^S_e)\quad\text{for}\quad N^L_e\geqslant N^S_e, \tag{9}$$

since the Landau levels with different N in the same conduction subband do not cross.[26] Hence, the necessary condition (not sufficient) for a Stokes Raman process is

$$\Delta N^L + \Delta N^S \geqslant 0, \tag{10}$$

where $\Delta N^L = N_e^L - N_h^0$ and $\Delta N^S = N_h^0 - N_e^S$. Let us denote the net Landau level change in the conduction band as

$$\Delta N = N_e^L - N_e^S = \Delta N^L + \Delta N^S. \tag{11}$$

If the net Landau level change (10) equals zero ($\Delta N^L + \Delta N^S = 0$) the electron states involved in the absorption and emission are in the same Landau level. In this case, the measured Raman shift should correspond to the effective Zeeman splitting of the first conduction subband indicating a spin-flip Raman scattering process. It is important to noticed that there is a Landè factor sign restriction for spin-flip Raman scattering processes. This effect will be discussed in Sec. V.

We have to emphasize that different scattering configurations will activate selectively different excitation states depending on their symmetry properties. In this study we consider two major configurations. One corresponds to the incoming light along the z direction with circular polarization (denoted by $\sigma^{\pm}$) and the scattered light collected on the x direction, with linear polarization z [in Porto's notation $z(\sigma_L^{\pm},z)x$]. The signs $\pm$ indicate the direction of rotation of circularly polarized light, with polarization vector $\mathbf{e}^{\pm} = (e_x \pm i e_y)/\sqrt{2}$. The other configurations here studied involve back-scattering processes in Faraday geometry $z(\sigma_L^{\pm},\sigma_S^{\pm})\overline{z}$ and $z(\sigma_L^{\pm},\sigma_S^{\mp})\overline{z}$.

For σ_L^+ or σ_S^-, the matrix elements in Eq. (8) are given by

$$\begin{aligned}\langle N_{i'},\mathrm{I}|V|N_i,\mathrm{I}\rangle = \frac{iP}{\sqrt{3}}\langle N_\alpha|e^{\pm i\kappa_\perp \rho}|N_\beta\rangle[(&\langle A_1^{i'}|\cos\kappa_z z|A_7^i\rangle \\ &+ \sqrt{2}\langle A_1^{i'}|\cos\kappa_z z|A_8^i\rangle \\ &- \sqrt{2}\langle B_4^{i'}|\cos\kappa_z z|B_5^i\rangle \\ &- \langle B_3^{i'}|\cos\kappa_z z|B_5^i\rangle)\,\delta_{N_\alpha,N'-1}\delta_{N_\beta,N} \\ &- \sqrt{3}\langle A_2^{i'}|\cos\kappa_z z|A_1^i\rangle\,\delta_{N_\alpha,N'-2}\delta_{N_\beta,N-1} \\ &- \sqrt{3}\langle B_5^{i'}|\cos\kappa_z z|B_6^i\rangle\,\delta_{N_\alpha,N'}\delta_{N_\beta,N+1}],\end{aligned} \tag{12}$$

where $iP = i\langle s|p_z|x\rangle$. In the case of incident (scattered) light κ corresponds to $\kappa^L(-\kappa^S)$. For σ_L^- or σ_S^+ the corresponding matrix elements are obtained from the Hermitian adjoint of Eq. (12).

The matrix elements $\langle N_{i'},\mathrm{II}|V|N_i,\mathrm{II}\,t\rangle$ can be obtained by interchanging $A_i \leftrightarrows B_i$ on both sides of the $\cos\kappa_z z$ in Eq. (12). The elements $\langle N_{i'},\mathrm{II}|V|N_i,\mathrm{I}\rangle$ are given by replacing $\cos\kappa_z z \to i\sin\kappa_z z$ and interchanging $A_i \leftrightarrows B_i$ on the left side of the $\sin\kappa_z z$. Finally, for $\langle N_{i'},\mathrm{I}|V|N_i,\mathrm{II}\rangle$ we replace $\cos\kappa_z z \to i\sin\kappa_z z$ and $A_i \leftrightarrows B_i$ on the right side.

In the case of linear polarization z the matrix elements are given by

$$\begin{aligned}\langle N_{i'},\mathrm{I}|V|N_i,\mathrm{I}\rangle = \frac{iP}{\sqrt{3}}\langle N_\alpha|e^{\pm i\kappa_\perp \rho}|N_\beta\rangle[(&\sqrt{2}\langle A_1^{i'}|\cos\kappa_z z|A_3^i\rangle \\ &- \langle A_1^{i'}|\cos\kappa_z z|A_4^i\rangle + \sqrt{2}\langle B_3^{i'}|\cos\kappa_z z|B_1^i\rangle \\ &- \langle B_4^{i'}|\cos\kappa_z z|B_1^i\rangle)\,\delta_{N_\alpha,N'-1}\delta_{N_\beta,N-1} \\ &\times(\sqrt{2}\langle A_5^{i'}|\cos\kappa_z z|A_7^i\rangle + \langle B_5^{i'}|\cos\kappa_z z|B_8^i\rangle \\ &+ \sqrt{2}\langle B_7^{i'}|\cos\kappa_z z|B_5^i\rangle + \langle B_8^{i'}|\cos\kappa_z z|B_5^i\rangle)].\end{aligned} \tag{13}$$

For the other matrix elements we have to proceed in the same way as indicated for the case of circular polarization. The dependence on $\kappa_\perp$ in Eqs. (12) and (13) is given by

$$|\langle N'|e^{i\kappa_\perp \rho}|N\rangle|^2 = e^{-Q^2}(Q^2)^{\Delta}\left\{\min\left(\sqrt{\frac{N'!}{N!}},\sqrt{\frac{N!}{N'!}}\right)L_{\min(N',N)}^{|\Delta|}(Q^2)\right\}^2, \tag{14}$$

where $Q^2 = \lambda^2\kappa_\perp^2/2$, λ is the magnetic length, $L_n^m(x)$ is the generalized Laguére polynomial, and

$$\Delta \equiv |N' - N|. \tag{15}$$

The quantity Δ defines the order of the matrix elements on Q^2. Terms similar to those in Eq. (14) appear twice in Eq. (8), once due to incoming light with $Q_L^2 = \lambda^2\kappa_\perp^{L2}/2$ and the other as function of $Q_S^2 = \lambda^2\kappa_\perp^{S2}/2$ that corresponds to the scattered light.

A. Dipole approximation

For interband optical transitions, the carrier-light interaction is usually treated within the dipole approximation ($\kappa = 0$). Because the term given by Eq. (14) is proportional to $e^{-Q^2}(Q^2)^{\Delta}$, the dipole approximation (with $\kappa_\perp = \kappa_z = 0$) allows for transitions with $\Delta = 0$ only. All the terms with $\sin(\kappa_z z)$ and $\Delta \neq 0$ vanish [see Eqs. (12) and (13)]. In a parabolic band model, the condition $\Delta = |N' - N| = 0$ for an optical transition would restrict the transitions to those with $N_{i'} = N_i$, since the parabolic terms are diagonal. Any optical transition with $N_{i'} \neq N_i$ is the result of inter Landau level mixing. In a multiband model the condition $\Delta = 0$ does not necessarily means that $N_{i'} = N_i$.

The selection rules for the optical transitions resulting from a multiband model are thus considerably relaxed in comparison to the selection rules obtained from a parabolic band model. For instance, a transition $\langle N'_{e\downarrow}|V^{\sigma^+}|N_{hh\uparrow}\rangle$ is forbidden in a parabolic model because $\langle e\downarrow|\mathbf{e}\cdot\mathbf{p}^+|hh\uparrow\rangle = 0$. However, in the multiband model, it is given by

TABLE I.

$z(\sigma_L^{\pm},z)x$				$z(\sigma_L^{+},\sigma_S^{-})\overline{z}$	
transition	$\sigma_L^{+}(\sigma_L^{-})$	transition	z	transition	σ_S^{-}
$hh\uparrow\rightarrow e\uparrow$	$\Delta N^L=2(-)$	$e\downarrow\rightarrow hh\uparrow$	$\Delta N^S=-2$[a]	$e\uparrow\rightarrow hh\uparrow$	$\Delta N^S=0$
$hh\downarrow\rightarrow e\downarrow$	$\Delta N^L=0(-2$[b]$)$	$e\uparrow\rightarrow hh\downarrow$	$\Delta N^S=2$	$e\downarrow\rightarrow hh\downarrow$	$\Delta N^S=2$
$lh\downarrow\rightarrow e\uparrow$	$\Delta N^L=0(-)$	$e\downarrow\rightarrow lh\downarrow$	$\Delta N^S=0$*	$e\uparrow\rightarrow lh\downarrow$	$\Delta N^S=2$
$lh\uparrow\rightarrow e\downarrow$	$\Delta N^L=2(0$[b]$)$	$e\uparrow\rightarrow lh\uparrow$	$\Delta N^S=0$	$e\downarrow\rightarrow lh\uparrow$	$\Delta N^S=0$

[a]Such a process is not effective if $g<0$.
[b]Such a process is not effective if $g>0$.

$$\langle N'_{e\downarrow}|V^{\sigma^+}|N_{hh\uparrow}\rangle \sim -iP\langle B_5^{i'}|\cos\kappa_z z|B_6^{i}\rangle\langle N'|e^{i\kappa_\perp \rho}|N+3\rangle,$$

which does not vanish in the dipole approximation for $N'-N=3$. The existence of a component $|u_6\rangle=|u_{hh\downarrow}\rangle$ in the state $|N_{hh\uparrow}\rangle$ is the result of the hybridization of the valence band levels as revealed in Figs. 2(b) and 2(c). For crossed polarizations as $z(\sigma_L^{\pm},z)x$ or $z(\sigma_L^{+},\sigma_S^{-})\overline{z}$ the dipole approximation can be used to describe ERRS processes. The ERRS selection rules for crossed polarizations are given in Table I. The 8×8 $\mathbf{k}\cdot\mathbf{p}$ Hamiltonian model does not preserve the Landau level index for the optical transitions in the dipole approximation. It is remarkable that spin-flip Raman processes with $\Delta N=0$ are allowed in the configurations $z(\sigma_L^{\pm},z)x$. This important fact shows that the measured Raman shift for those transitions with $\Delta N=0$ corresponds to the effective Zeeman splitting and it can be useful for the determination of the effective Landè factor and to study its dependence on the magnetic field and QW parameters. The obtained ERRS selection rules are quite general and bound to the condition in Eq. (10) ($\Delta N^L+\Delta N^S\geqslant 0$). In the particular case of $\Delta N^L+\Delta N^S=0$ we obtained restrictions to the allowed Stokes transitions depending on the Landè factor sign (see Sec. V).

In backscattering configurations for parallel circular polarizations of both incident and scattered light $z(\sigma_L^{\pm},\sigma_S^{\pm})\overline{z}$ ERRS processes are forbidden within the dipole approximation because all optical transitions involve terms proportional to $\sin(\kappa_z z)$. Then, we have to go beyond this approximation and take into account the finite values of the incident and scattered light wave vectors.

B. Beyond dipole approximation

At $\boldsymbol{\kappa}\neq 0$, ERRS processes for backscattering in Faraday configuration with parallel polarizations $z(\sigma_L^{\pm},\sigma_S^{\pm})\overline{z}$ are allowed. For finite value of the light wave vector $\boldsymbol{\kappa}$ the above obtained selection rules (Table I) are relaxed and transitions within the first QW subband are possible. In the backscattering configuration we have strictly perpendicular incidence with $\theta=0°$, $\kappa_\perp^S=\kappa_\perp^L=0$, but $\kappa_z=\eta/c(\omega_L+\omega_S)$. In this limit $Q_S=Q_L=0$ and the matrix elements given by Eq. (14) are again different from zero only if $\Delta=0$, which provides the selection rules for the Landau level index N. This case will be called the ''the first order approximation'' since it comes out when terms proportional to $\sin(\kappa_z z)$ are considered within the first order on κ_z. The corresponding Raman selection rules and interband transitions are listed in Table II.

It is important to remark that at $\boldsymbol{\kappa}\neq 0$ the Raman selection rules for crossed polarization $z(\sigma_L^{+},\sigma_S^{-})\overline{z}$ shown in Table I are also relaxed and new interband transitions for ΔN^L and ΔN^S appear in the Raman spectrum. Nevertheless, the corresponding intensities are weak in comparison to those found in the framework of the dipole approximation. For sake of shortness the corresponding selection rules for backscattering configuration with crossed polarization when the light wave vector is assumed different from zero will not be listed. Moreover, there are configurations, such as $z(\sigma_L^{-},\sigma_S^{+})z$, in which intrasubband transition in both the dipole and the first order approximation is forbidden. The main restriction in both approximations comes from the rule defined in Eq. (10). For instance, both the transitions $hh\downarrow\sigma_L^{-}{}_{\rightarrow}e\downarrow$ with $\Delta N^L=-2$ and $e\downarrow\sigma_S^{+}{}_{\rightarrow}hh\downarrow$ with $\Delta N^S=0$ are allowed within the dipole approximation, but they do not participate in a Stokes Raman process since $\Delta N^L+\Delta N^S=-1<0$. Any combination of transitions out of Tables I and II, for $z(\sigma_L^{-},\sigma_S^{+})\overline{z}$ geometry, is forbidden in both the dipole and the first order approximation for analogous reasons.

If the incoming (scattered) light in Faraday configuration is not strictly perpendicular to the well interfaces, but it has rather a small angle θ, a small component of the light momentum lies within the xy plane with $\kappa_\perp=\kappa\sin\theta$. Following Eq. (14), the next order approximation will contain terms proportional to Q^2 and we have to consider all possible combinations of the matrix elements (14) either proportional to Q_L^2 or Q_S^2, which involve transitions with $\Delta=|N'-N|=1$. Typical Raman measurements have already been performed with an effective wave vector transfer parallel to the QW

TABLE II. ERRS selection rules beyond the dipole approximation for backscattering in the Faraday configuration with circular parallel polarizations. Only the first valence and conduction QW subbands are considered.

	$z(\sigma_L^{\pm},\sigma_S^{\pm})\overline{z}$		
transition	$\sigma_L^{+}(\sigma_L^{-})$	transition	$\sigma_S^{+}(\sigma_S^{-})$
$hh\downarrow\rightarrow e\downarrow$	$\Delta N^L=0(-2)$	$e\uparrow\rightarrow hh\downarrow$	$\Delta N^S=1(3)$
$hh\uparrow\rightarrow e\downarrow$	$\Delta N^L=3(1)$	$e\uparrow\rightarrow hh\uparrow$	$\Delta N^S=-2(0)$
$lh\downarrow\rightarrow e\downarrow$	$\Delta N^L=1(-1)$	$e\uparrow\rightarrow lh\downarrow$	$\Delta N^S=0(2)$
$lh\uparrow\rightarrow e\downarrow$	$\Delta N^L=2(1)$	$e\uparrow\rightarrow lh\uparrow$	$\Delta N^S=-1(1)$

TABLE III. ERRS selection rules beyond the dipole approximation for small angel for the incidence or scattered light in Faraday configuration with circular crossed polarization. Only the first valence and conduction QW subbands are considered. Bold numbers in ΔN indicate those transitions proportional to Q_S^2.

	$z(\sigma_L^-,\sigma_S^+)\bar{z}$		
transition	σ_L^-	transition	σ_S^+
$hh\downarrow\rightarrow e\downarrow$	$\Delta N^L=\mathbf{-1}$ or -2	$e\uparrow\rightarrow hh\downarrow$	$\Delta N^S=1$ or **3**
$hh\uparrow\rightarrow e\downarrow$	$\Delta N^L=\mathbf{2}$ or 1	$e\uparrow\rightarrow hh\uparrow$	$\Delta N^S=-2$ or **0**
$lh\downarrow\rightarrow e\downarrow$	$\Delta N^L=\mathbf{0}$ or -1	$e\uparrow\rightarrow lh\downarrow$	$\Delta N^S=0$ or **2**
$lh\uparrow\rightarrow e\downarrow$	$\Delta N^L=\mathbf{1}$ or 0	$e\uparrow\rightarrow lh\uparrow$	$\Delta N^S=-1$or **1**

layers ($\kappa_\perp\neq 0$) using a rotating sample.[28,29] Table III indicates the allowed processes in the configuration $z(\sigma_L^-,\sigma_S^+)\bar{z}$ due to Q^2 contributions. It is important to point out that our theoretical approach is valid only for small angles of the incident light inside the sample since we have not considered the corresponding rotation of the polarization vectors in the calculations, leaving unchanged the optical matrix elements $\Pi_{j'j}^{\sigma}=\langle u_{j'}|\mathbf{e}\cdot\mathbf{p}|u_j\rangle$ as for $\theta=0$. According to these selection rules given in Table III any allowed process has spin-flip nature with $\Delta N=\Delta N^L+\Delta N^S=0$.

Up to this point, we can see from Tables I, II, and III that the most common processes in all approximations and different scattering configurations are of the type

$$vb\rightarrow e\downarrow-e\uparrow\rightarrow vb \quad \text{or} \quad vb\rightarrow e\uparrow-e\downarrow\rightarrow vb. \tag{16}$$

All these processes are related to spin-flip transitions in the first conduction subband where $\Delta N=0$ or $\Delta N\neq 0$.

V. DISCUSSION

The ERRS selection rules described by the resonant theory presented here indicate that the spin splitting of the conduction band shows up at small Raman shift (see Fig. 2). According to these selection rules and from the position of the corresponding resonances in the Raman spectrum one is able to determine the structure of the spin-split electronic subbands. A remarkable fact is that the breaking of the ERRS selection rules (obtained in the framework of parabolic Hamiltonian model[10]), induced by the interband coupling, allows for the detailed study of electronic properties exclusively related to the behavior of the electrons in the lowest conduction subband.

First, we would like to discuss the allowed transition in Faraday configuration and the physical processes we can extract from the ERRS cross section as a function of the magnetic field and electron concentration. In Fig. 3, we show several diagrams that correspond to those allowed transitions detailed in Tables I, II, and III. It can be noticed that the processes shown in Fig. 3 contain complementary information. For instance, the difference between the Raman shift of the processes of the diagrams 3(a) and 3(b) (denoted $E_{\text{shift}}^{(a)}$ and $E_{\text{shift}}^{(b)}$, respectively)

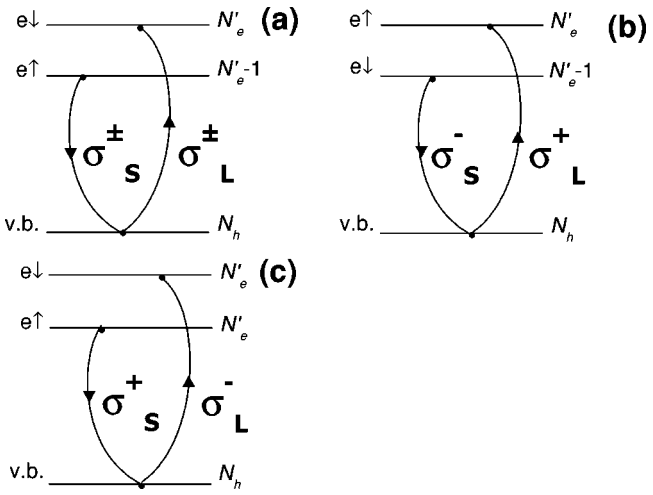

FIG. 3. ERRS diagrams for different scattering configurations (a) $z(\sigma_L^{\pm},\sigma_S^{\pm})\bar{z}$, (b) $z(\sigma_L^-,\sigma_S^+)\bar{z}$, (c) $z(\sigma_L^+,\sigma_S^-)\bar{z}$.

$$\begin{aligned}E_{\text{shift}}^{(a)}-E_{\text{shift}}^{(b)}&=[\varepsilon_{e\downarrow}(N')-\varepsilon_{e\uparrow}(N'-1)]-[\varepsilon_{e\uparrow}(N')-\varepsilon_{e\downarrow}(N'-1)]\\&=[\varepsilon_{e\downarrow}(N')-\varepsilon_{e\uparrow}(N')]+[\varepsilon_{e\downarrow}(N'-1)-\varepsilon_{e\uparrow}(N'-1)]\\&=-[g(N')+g(N'-1)]\mu_B B_0,\end{aligned} \tag{17}$$

is proportional to the mean effective Landè factor g of the consecutive Landau levels, which is independent of the sign of $g(N)$.

In order to highlight the influence of the band coupling and the results coming from a detailed microscopic theory using a 8×8 $\mathbf{k}\cdot\mathbf{p}$ model, we selected a narrow gap $Hg_{0.8}Cd_{0.2}Te/CdTe$ QW and the Raman scattering cross section was calculated at $\hbar\omega_L=400$ meV for a 100 Å well width. The Raman cross-section calculation for the configuration $z(\sigma_L^+,\sigma_S^+)\bar{z}$ is shown in Fig. 4(a) for $n_{2\,\text{D}}=0.72\times 10^{12}$ cm^{-2}. The magnetic fields are chosen in such a way that the filling factor varies from 4 to 3. The resonances labeled A and B correspond to processes such as diagram (a) of Fig. 3. The effective Landau level difference is $\Delta N=1$ for all transitions ($vb\rightarrow e\downarrow-e\uparrow\rightarrow vb$, see Table II). Peaks A represent processes with a photon emission from the electron Landau level $N_e^S=1$ while peak B to an outgoing process with $N_e^S=0$. The interchange of strength of the peaks A and B with the magnetic field (or filling factor) is associated to jumps of the Fermi level at integer values of the filling factor ν. In this case each resonance survives at intervals $\Delta\nu=4$ since we deal with transitions $vb\rightarrow e\downarrow-e\uparrow\rightarrow vb$ with $\Delta N=1$. The filling factor interval $\Delta\nu$ where the process $vb\rightarrow\alpha-\beta\rightarrow vb$ survives is an indication of the number of Landau levels that can be occupied between the states $\alpha-\beta$ (including themselves). The transition becomes statistically effective when the state denoted β is partially or totally occupied while the state α is unoccupied or partially occupied. For negative Landè g factors there are four levels within the interval $[e\downarrow(N+1)-e\uparrow(N)]$. The state $e\uparrow(N)$ starts to be occupied at even values $\nu=2k$, $k=0,1,\ldots$ (lower limit of the filling factor interval) and the state

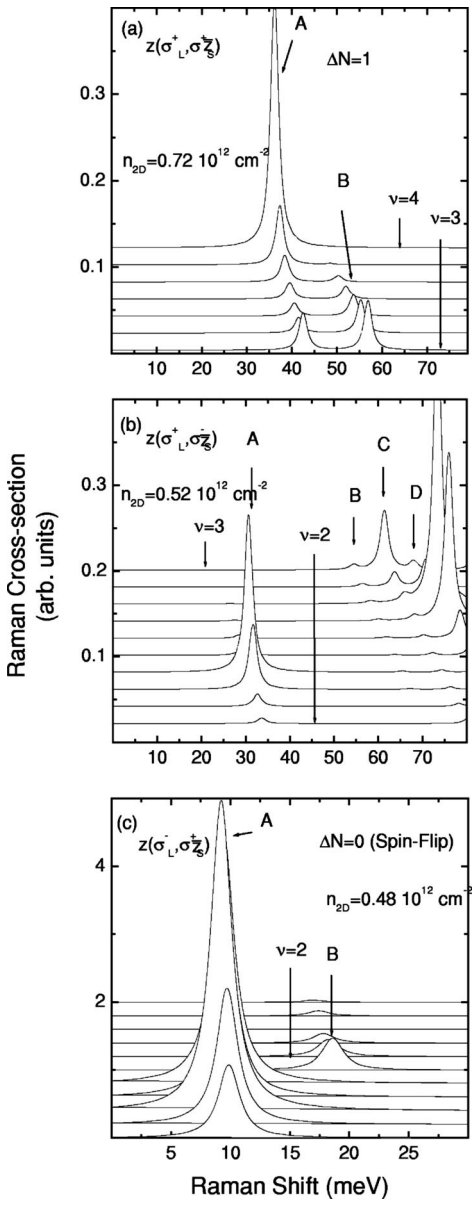

FIG. 4. Calculated Raman scattering cross section in Faraday configuration. (a) $z(\sigma_L^+,\sigma_S^+)\bar{z}$ geometry and $n_{2\,\mathrm{D}}=0.72\times10^{12}\ \mathrm{cm}^{-2}$. Peaks A and B represent processes with $N_e^S=1$ and 0, respectively. (b) $z(\sigma_L^+,\sigma_S^-)\bar{z}$ configuration and $n_{2\,\mathrm{D}}=0.52\times10^{12}\ \mathrm{cm}^{-2}$. Structure A shows resonant transitions from $N_e^S=1$ and effective Landau level difference $\Delta N=1$. Peak B corresponds to $N_e^S=3$ and C, D to outgoing transitions from $N_e^S=2$. This three structures have effective Landau level difference $\Delta N=2$. (c) $z(\sigma_L^-,\sigma_S^+)\bar{z}$ geometry and $n_{2\,\mathrm{D}}=0.48\times10^{12}\ \mathrm{cm}^{-2}$. In the calculation the value of $\kappa_\perp=4\times10^4\ \mathrm{cm}^{-1}$ is used. Peaks A and B show outgoing transitions with $N_e^S=1$ and 0, respectively with $\Delta N=0$.

$e\downarrow(N+1)$ becomes totally occupied at $\nu=2k+4$ (upper limit), when the transition is statistically forbidden. A resonant transition fades away once both conduction band levels involved in the absorption and the emission of light become totally occupied [see Eq. (6)].

A more complex picture is obtained for the Raman cross section for back scattering with cross polarizations $z(\sigma_L^+,\sigma_S^-)\bar{z}$, beyond the dipole approximation when the filling factors ranges between 3 and 2 as shown in Fig. 4(b). As in the previous case, peak A corresponds to an inter-Landau level process $vb\rightarrow e\uparrow-e\downarrow\rightarrow vb$ shown in Fig. 3 diagram (b) with $\Delta N=\Delta N^L+\Delta N^S=1$ and outgoing scattering from $N_e^S=1$. The peaks B, C, and D in Fig. 4(b) correspond to transitions that conserve the spin with $\Delta N=2$. Structures B represent processes $(vb\rightarrow e\uparrow-e\uparrow\rightarrow vb)$ with outgoing transitions from $N_e^S=3$, C is related to processes $(vb\rightarrow e\downarrow-e\downarrow\rightarrow vb)$ with $N_e^S=2$, while peaks D give us transitions $(vb\rightarrow e\uparrow-e\uparrow\rightarrow vb)$ also with $N_e^S=2$. At low fields, for low Landau levels, in the particular selection of the QW parameters considered here, with negative Landè factor, the states $|e\uparrow,N_e+1\rangle$ and $|e\downarrow,N_e\rangle$ are very close to each other [see Fig. 2(a)] leading to a Raman shift near the value of the Zeeman splitting. We need to emphasize that the spin-flip intra-Landau-level transition $(\Delta N=0)$ can be identified by tuning the filling factor. At even values of the filling factor both spin-split states of the same Landau level are totally occupied and the spin-flip intraband level transition is forbidden. Hence, this process is allowed between two consecutive even values of the filling factor. In Fig. 4(b) it can be seen that the peak A fades at odd values of the filling factor, so it cannot be associated with the spin-flip transitions with $\Delta N=0$ (see Ref. 30). In conclusion, the resonances labeled A in Figs. 4(a) and 4(b) obtained by two independent scattering configurations can be used to determine the mean effective Landè factor from Eq. (17) with $N_e=1$. The peaks B, C, and D in Fig. 4(b) correspond to transitions that conserve the spin with $\Delta N=2$. The resonances labeled A in Figs. 4(a) and 4(b) obtained by two independent scattering configurations can be used to determine the mean effective Landè factor from Eq. (17) with $N_e=1$.

In the framework of the Faraday scattering geometry, let us discuss the selection rules given in Table III and related to the $z(\sigma_L^-,\sigma_S^+)\bar{z}$ scattering configuration. The transitions as represented in diagram (c) of Fig. 3 are allowed in $z(\sigma_L^-,\sigma_S^+)\bar{z}$ geometry within the second order approximation on $\kappa_\perp$. In this particular case, intrasubband transitions are forbidden within the dipole or the first order approximations on $\kappa_\perp$. In the calculations the value $\kappa_\perp=4\times10^4\ \mathrm{cm}^{-1}$ is used. The peaks labeled A and B in Fig. 4(c) represent spin-flip processes $(vb\rightarrow e\downarrow-e\uparrow\rightarrow vb)$ with effective Landau level difference $\Delta N=0$ and outgoing transitions from $N_e=1$ and $N_e=0$, respectively. In this case the Raman shift in both cases corresponds exactly to the effective Zeeman splitting

$$E_{\mathrm{shift}}=\varepsilon_{e\downarrow}(N')-\varepsilon_{e\uparrow}(N')=-g(N')\mu_B B_0. \qquad (18)$$

This result is different from the one obtained in the complementary configurations shown in Figs. 4(a) and 4(b). Notice the evolution of the resonant picture with the magnetic field (or filling factor) in Fig. 4(c). As pointed out before, the resonances fade away at even values of the filling factor for spin-flip intra-Landau level transitions. The filling factor modulation may serve as a tuning tool which selectively activates resonant scattering channels depending on the magnetic field, electron concentration, and spin of the involved electronic states.

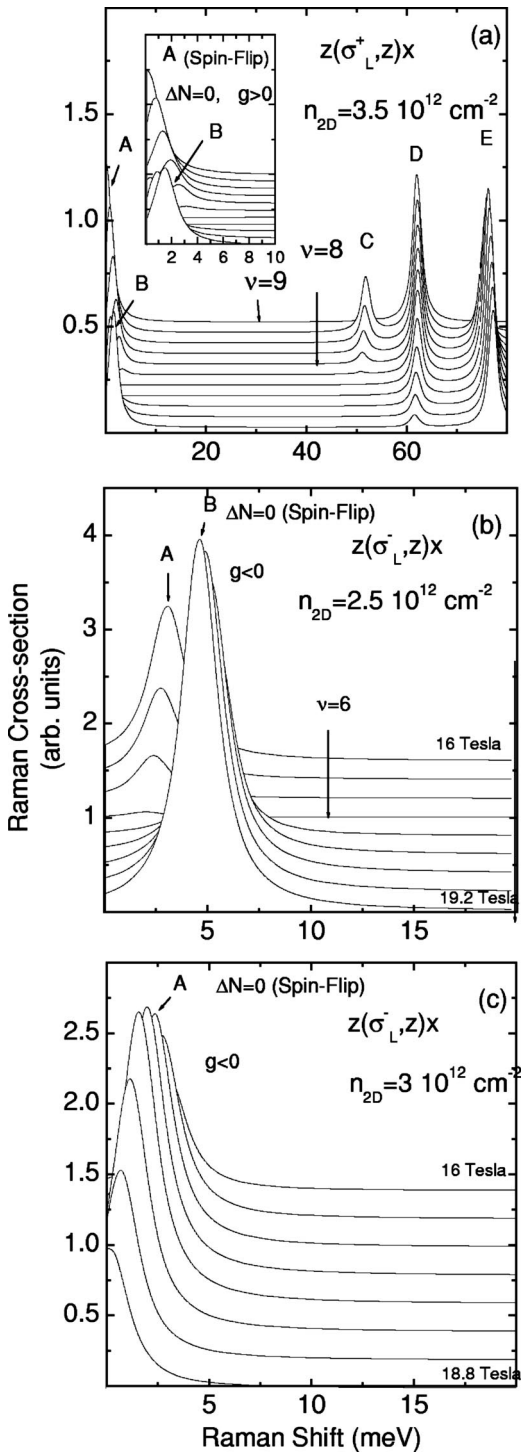

FIG. 5. ERRS cross section in crossed polarizations within the dipole approximation as a function of the applied magnetic field. Scattering processes $vb \rightarrow e\downarrow - e\uparrow \rightarrow vb$ are represented (see Table I). (a) $z(\sigma_L^+,z)x$ configuration with $n_{2\,\mathrm{D}}=3.5\times10^{12}$ cm^{-2}. Spin-flip transitions with effective Landau level difference $\Delta N=0$, $N_e^S=4$ (peaks A), and $N_e^S=3$ (peaks B). Peaks labeled by C, D, and E correspond to outgoing transitions from $N_e^S=4$, 3, and 2, respectively, and $\Delta N=2$. (b) $z(\sigma_L^-,z)x$ configuration with $n_{2\,\mathrm{D}}=2.5\times10^{12}$ cm^{-2}. (c) $z(\sigma_L^-,z)x$ configuration with $n_{2\,\mathrm{D}}=3\times10^{12}$ cm^{-2}. Labels A and B represent spin-flip processes, $\Delta N=0$, with outgoing transitions from $N_e^S=3$ and $N_e^S=2$.

VI. LANDÈ FACTOR SIGN INVERSION

Interesting results are obtained in the Raman scattering process when circular and linear polarizations are combined, i.e., $z(\sigma_L^+,z)x$ and $z(\sigma_L^-,z)x$ scattering configurations. As we pointed out in Sec. IV A the inelastic response of a QW in a magnetic field is asymmetric. This is clearly indicated in Figs. 5(a) and 5(b), where the processes of type $vb \rightarrow e\downarrow - e\uparrow \rightarrow vb$ with $\Delta N=2$ together with spin-flip transitions $vb \rightarrow e\uparrow - e\downarrow \rightarrow vb$ with $\Delta N=0$ are active in the configuration $z(\sigma_L^+,z)x$. However in the configuration $z(\sigma_L^-,z)x$, shown in Fig. 5(b), only spin-flip transitions $vb \rightarrow e\downarrow - e\uparrow \rightarrow vb$ with $\Delta N=0$ appear. In Fig. 5(a) the peaks labeled by A and B represent spin-flip transitions with effective Landau level difference $\Delta N=0$ outgoing from Landau levels $N_e^S=4$ and 3, respectively, while peaks C, D, and E are due to scattering processes with $N_e^S=4$, 3, and 2, and $\Delta N=2$. Figure 5(b) shows spin-flip transitions with $N_e^S=3$ (peaks A), $N_e^S=2$ (peaks labeled by B), and effective Landau level difference $\Delta N=0$.

The inelastic response is also very sensitive to the two-dimensional electron density. Variations in the occupation of the Landau levels may lead to drastic changes of the Raman spectra as can be seen in Fig. 5(c) for the $z(\sigma_L^-,z)x$ configuration but $n_{2\,\mathrm{D}}=3\times10^{12}$ cm^{-2}. The most relevant difference between configurations $z(\sigma_L^+,z)x$ and $z(\sigma_L^-,z)x$ is that the spin-flip transitions in both considered cases correspond to opposite signs of the effective g Landè factor. In the configuration $z(\sigma_L^+,z)x$ the spin-flip transition is allowed for positive Landè factors. Notice in Fig. 2(a) that $g>0$ is reached for Landau levels $N_e>2$ and high fields. In the inset of Fig. 5(a) it can be clearly seen that the Raman shift for the spin-flip resonances A and B move away from zero as the magnetic field increases. The zero value of the Raman shift corresponds to the crossing point of the spin-split levels in the

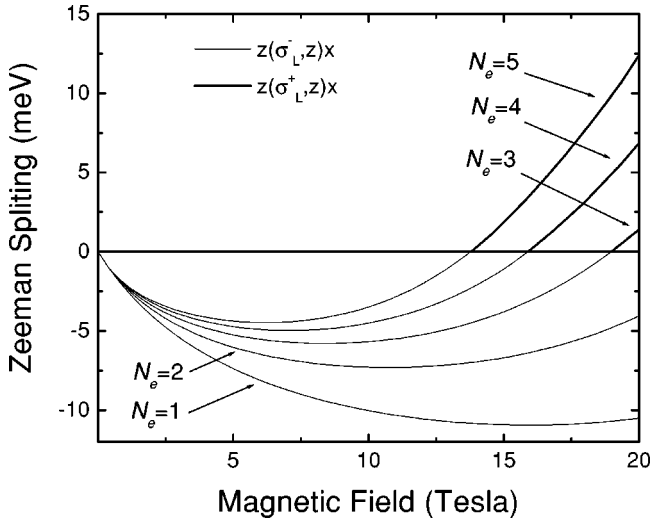

FIG. 6. Calculated Zeeman splitting for different Landau levels in the first conduction subband. The solid thick lines represent the values of the Raman shift according to ERRS scattering configuration $z(\sigma_L^+,z)x$ while the solid thin lines represent those obtained in the $z(\sigma_L^-,z)x$ geometry.

first conduction subband [see Fig. 2(a)]. On the other hand, in the configuration $z(\sigma_L^-,z)x$ [Figs. 5(b) and 5(c)], the spin-flip Raman shift comes closer to zero as the magnetic field increases. These Raman processes, in turn, are allowed for negative Landè factor. Both scattering configurations are complementary providing the negative and positive values of the Landè factors following the magneto fan plot of Fig. 2(a). The corresponding Zeeman splitting obtained from the two cross polarization configurations mentioned above is shown in Fig. 6. The strong dependence of the Zeeman splitting on the Landau level index and magnetic field is the result of the strong intersubband coupling. We remark once more that the simple parabolic band model would give a linear dependence on the magnetic field and independence on the Landau level index N_e. The interband mixing turns out to be crucial for the anomalous behavior of the Landè factor in QW's as reported recently both theoretically[27] and experimentally.[31]

VII. CONCLUSIONS

We showed that the Raman cross section in the resonant regime along with a proper introduction of the interband coupling explains the appearance of spin-flip Raman scattering in the different configurations considered in this work. The selection rules were obtained for transitions within the first valence and conduction subband of hybridized electronic states based on the 8×8 Kane-Weiler Hamiltonian model. The relaxation of the selection rules, induced by the intersubband coupling, provokes an asymmetric Raman response. Using different scattering configurations one obtains complementary information about the electronic band structure and symmetry properties of the corresponding electronic states. Interesting effects, such as the anomalous crossing of Landau levels in the first conduction subband, can be studied by using spin-flip Raman scattering. The magnetic field dependence of the Fermi level (or the filling factor) introduces an effective tuning mechanism for the resonant inelastic response and can be used as a tool to identify the levels involved in the resonant transitions.

ACKNOWLEDGMENTS

This work was supported by FAPESP and CNPq, Brazil.

[1] F. A. Blum, Phys. Rev. B **1**, 1125 (1970).
[2] *Light Scattering Spectra of Solids*, edited by G. B. Wright (Springer-Verlag, New York 1969).
[3] P. A. Wolff, Phys. Rev. Lett. **16**, 225 (1966); Phys. Rev. **171**, 436 (1968).
[4] Y. Yafet, Phys. Rev. **152**, 858 (1966).
[5] S. S. Jha, Phys. Rev. **179**, 764 (1969).
[6] D. Richards, Phys. Rev. **61**, 7517 (2000).
[7] D. W. Wang and S. Das Sarma, Phys. Rev. B **65**, 125322 (2002).
[8] V. López-Richard, G.-Q. Hai, G. E. Marques, and C. Trallero-Giner, Phys. Rev. B **66**, 155303 (2002).
[9] W. Walukiewicz, Phys. Rev. B **22**, 3957 (1980).
[10] *Light Scattering in Solids IV*, edited by M. Cardona and G. Günterodt (Springer-Verlag, Berlin, 1984).
[11] S. Das Sarma and D. W. Wang, Phys. Rev. Lett. **83**, 816 (1999).
[12] A. G. Mal'shukov, K. A. Chao, and M. Willander, Phys. Rev. B **55**, 1918 (1997).
[13] V. A. Froltsov, A. G. Mal'shukov, and K. A. Chao, Phys. Rev. B **60**, 14 255 (1999).
[14] V. A. Froltsov, A. G. Mal'shukov, and K. A. Chao, Phys. Rev. B **64**, 073309 (2001).
[15] D. Richards and B. Jusserand, Phys. Rev. B **59**, 2506 (1999).
[16] O. Z. Karimov, D. Wolverson, J. J. Davies, S. I. Stepanov, T. Ruf, S. V. Ivanov, S. V. Sorokin, C. B. O'Donnell, and K. A. Prior, Phys. Rev. B **62**, 16 582 (2000).
[17] Y. G. Kusvarev, A. V. Houdinov, D. Wolverson, and J. Kossut, Phys. Status Solidi B **229**, 741 (2002).
[18] A. A. Sirenko, T. Ruf, M. Cardona, D. R. Yakovlev, W. Ossau, A. Waag, and G. Landwehr, Phys. Rev. B **56**, 2114 (1997).
[19] J. P. Sattler, B. A. Weber, and J. Nemarich, Appl. Phys. Lett. **25**, 491 (1974).
[20] B. A. Weber, J. P. Sattler, and J. Nemarich, Appl. Phys. Lett. **27**, 93 (1975).
[21] P. W. Kruse, Appl. Phys. Lett. **28**, 90 (1976).
[22] P. W. Kruse and J. F. Ready, in *Nonlinear Optical Effects in* $Hg_{1-x}Cd_xTe$, *Semiconductors and Semimetals*, edited by R. K. Willardson and A. C. Beer (Academic, New York, 1966), Vol. 16.
[23] K. Ortner, X. C. Zhang, A. Pfeuffer-Jescher, C. R. Becker, G. Landwehr, and L. W. Molenkamp, Phys. Rev. B **66**, 075322 (2002).
[24] K. Ortner, X. C. Zhang, S. Oehling, J. Gerschutz, A. Pfeuffer-Jescher, V. Hoch, C. R. Becker, G. Landwehr, and L. W. Molenkamp, Appl. Phys. Lett. **79**, 3980 (2001).
[25] M. H. Weiler, in *Magneto-optical Properties of* $Hg_{1-x}Cd_xTe/CdTe$ *Alloys*, *Semiconductors and Semimetals* (Ref. 22).
[26] V. López-Richard, G. E. Marques, and C. Trallero-Giner, Phys. Status Solidi B **231**, 263 (2002).
[27] V. López-Richard, G. E. Marques, and C. Trallero-Giner, Solid State Commun. **114**, 649 (2000); **115**, 515 (2000).
[28] G. Fasol, N. Mestres, H. P. Hughes, A. Fischer, and K. Ploog, Phys. Rev. Lett. **56**, 2517 (1986).
[29] D. S. Kainth, D. Richards, A. S. Bhatti, H. P. Hughes, M. Y. Simmons, E. H. Linfield, and D. A. Ritchie, Phys. Rev. B **59**, 2095 (1999).
[30] V. López-Richard, G. E. Marques, and C. Trallero-Giner, J. Appl. Phys. **89**, 6400 (2001).
[31] R. Kotyar and T. L. Reinecke, Phys. Rev. B **63**, 085310 (2001).